# *In vivo* resonant Raman measurement of macular carotenoid pigments in the young and the aging human retina

**Werner Gellermann, Igor V. Ermakov, Maia R. Ermakova, and Robert W. McClane**

*Department of Physics and Dixon Laser Institute, University of Utah, Salt Lake City, Utah 84112*

**Da-You Zhao and Paul S. Bernstein**

*Department of Ophthalmology and Visual Sciences, Moran Eye Center, University of Utah School of Medicine, Salt Lake City, Utah 84132*

Received November 9, 2001; accepted January 4, 2002

We have used resonant Raman scattering spectroscopy as a novel, noninvasive, *in vivo* optical technique to measure the concentration of the macular carotenoid pigments lutein and zeaxanthin in the living human retina of young and elderly adults. Using a backscattering geometry and resonant molecular excitation in the visible wavelength range, we measure the Raman signals originating from the single- and double-bond stretch vibrations of the $\pi$-conjugated molecule's carbon backbone. The Raman signals scale linearly with carotenoid content, and the required laser excitation is well below safety limits for macular exposure. Furthermore, the signals decline significantly with increasing age in normal eyes. The Raman technique is objective and quantitative and may lead to a new method for rapid screening of carotenoid pigment levels in large populations at risk for vision loss from age-related macular degeneration, the leading cause of blindness in the elderly in the United States. 

*OCIS codes:* 170.0170, 170.4470, 170.4580, 170.1610, 300.6450, 330.4300.

## 1. INTRODUCTION

It has been hypothesized that the macular carotenoid pigments lutein and zeaxanthin[1,2] might play a role in the treatment and prevention of age-related macular degeneration (AMD), the leading cause of blindness in the elderly in the United States.[3,4] Supportive epidemiological studies have shown that there is an inverse correlation between high dietary intakes and blood levels of lutein and zeaxanthin and risk of advanced AMD.[5,6] It has also been demonstrated that macular pigment levels can be altered through dietary manipulation[7,8] and that carotenoid pigment levels are lower in autopsy eyes from patients with AMD.[9,10] Recently the Age-Related Eye Disease Study demonstrated that high-dose supplementation with antioxidant vitamins and minerals (vitamin C, vitamin E, beta-carotene, and zinc) can lower the rate of progression to advanced AMD in high-risk patients.[11] Comparable randomized, placebo-controlled prospective clinical study data to support the lutein and zeaxanthin hypothesis are not yet available, however.

The spatial distribution of lutein and zeaxanthin in the human and monkey retina has been studied extensively. Spectroscopic studies of tissue sections of primate maculae (the central 5–6 mm of the retina) indicate that there are very high concentrations of carotenoid pigments in the Henle fiber layer of the fovea and smaller amounts in the inner plexiform layer.[12] Biochemical studies have demonstrated that in the foveal area zeaxanthin predominates over lutein by a 2:1 ratio, whereas in the peripheral retina the concentration of lutein and zeaxanthin drops as much as 100-fold relative to the center of the fovea, and the zeaxanthin:lutein ratio reverses to 1:2.[13,14] It is thought that the majority of the carotenoids in the foveal region are associated either with cones[15] or with Müller cells[16] and that the carotenoids of the peripheral retina are present in the rod outer segments.[17,18] High-spatial-resolution psychophysical studies appear to correlate well with these findings, showing basically a symmetric distribution of macular pigment density that peaks at the center of the fovea and decreases exponentially outward, with an average width of 1.03 deg at half-maximum in normal subjects.[19]

The mechanisms by which these two macular pigments, derived exclusively from dietary sources such as green leafy vegetables and orange and yellow fruits and vegetables, might protect against AMD is still unclear. These pigments are known to be excellent free-radical-scavenging antioxidants in a tissue at high risk of oxidative damage owing to the high levels of light exposure and to abundant highly unsaturated lipids.[3,4,20,21] In addition, since these molecules absorb in the blue–green spectral range, they act as filters that may attenuate photochemical damage and/or image degradation caused by short-wavelength visible light reaching the retina.[22]

There is considerable interest in the measurement of macular carotenoid levels noninvasively in the elderly population to determine whether low levels of macular pigment are associated with increased risk of AMD.[23] Currently the most commonly used noninvasive method for measuring human macular pigment levels is a subjec-

 

tive psychophysical heterochromatic flicker photometry test involving color intensity matching of one light beam aimed at the fovea and another aimed at the perifoveal area.[19] This method is time intensive and requires an alert, cooperative subject with good visual acuity, and it may exhibit high intrasubject variability when macular pigment densities are low or if significant macular pathology is present.[24] Thus the usefulness of this method for assessing macular pigment levels in the elderly population most at risk for AMD is severely limited. Nevertheless, researchers have used flicker photometry to investigate important questions such as variation of macular pigment density with age and diet. In a recent flicker photometry study, for example, the pigment density was found to increase slightly with age,[25] but two other studies found the opposite trend.[23,26]

A number of objective techniques for the measurement of macular pigment in the human retina have been explored recently as alternatives to the subjective psychophysical tests. The underlying optics principles of these techniques are based on either fundus-reflection or fundus-fluorescence (autofluorescence) spectroscopy. In traditional fundus reflectometry, which uses a light source with a broad spectral continuum, reflectance spectra of the bleached retina are measured separately for fovea and perifovea. The double-path absorption of macular pigment is extracted from the ratio of the two spectra by reproducing its spectral shape in a multiparameter fitting procedure that uses appropriate absorption and scattering profiles of the various fundus tissue layers traversed by the source light.[27–30] One of the imaging variants of fundus reflectometry uses a TV-based imaging fundus reflectometer with sequential, narrow-bandwidth light excitation over the visible wavelength range and digitized fundus images.[31] Another powerful variant uses a scanning laser ophthalmoscope,[32,33] (SLO), employing raster scanning of the fundus with discrete laser-excitation wavelengths to produce highly detailed information about the spatial distribution of macular pigments (and photopigments).[34–38] In autofluorescence spectroscopy, lipofuscin in the retinal pigment epithelium is excited by light within and outside the wavelength range of macular pigment absorption. By measuring the lipofuscin fluorescence levels for fovea and perifovea, one can obtain an estimate of the single-pass absorption of macular pigment.[39,40]

Autofluorescence measurements of macular pigments were recently carried out in a group of 159 subjects (ages 15–80, normal retinal status) and compared with reflectometry measurements. Also, in a small subgroup, the autofluorescence measurements were compared with heterochromatic flicker photometry measurements.[40] Average macular pigment optical densities for the whole age group were $0.48 \pm 0.16$ for autofluorescence (2-deg test field), $0.23 \pm 0.07$ for reflectometry (2-deg test field), and $0.37 \pm 0.26$ for the psychophysical measurement (0.8-deg test field). Furthermore, autofluorescence was found to measure densities reproducibly to within 9% of the mean density, which is superior to the reproducibility obtained by reflectometry (22%) and flicker photometry (15–35% depending on age, training, and experience of subjects). In another recent study that compared reflectometry, SLO, and flicker photometry in the measurement of macular lutein uptake, SLO was found to be superior to spectral fundus reflectance, whereas psychophysical measurements yielded widely varying results.[30,41]

We investigated Raman scattering as a new approach[42,43] for the measurement of macular pigment levels in human subjects.[44,45] The technique described in this paper is objective as well as noninvasive and appears to be fast and quantitative; its exquisite specificity means that it could be used for patients with a variety of ocular pathologies. Thus this technique holds potential for a major advance in the study and possible prevention of macular degenerative diseases. Moreover, the noninvasive measurement of carotenoids by resonance Raman spectroscopy has even wider uses as a potential early diagnostic test of disorders in other human tissues such as the skin and the oral cavity.[46,47]

## 2. OPTICAL PROPERTIES AND RAMAN SCATTERING OF CAROTENOIDS IN SOLUTIONS

Carotenoids are $\pi$-electron conjugated carbon-chain molecules ($C_{40}H_{56}$) and are similar to polyenes regarding their structure and optical properties. Figure 1 shows the molecular structures for the three carotenoid pigment species $\beta$-carotene, zeaxanthin, and lutein. All three molecules contain nine alternating conjugated carbon double and single bonds that constitute a polyene backbone, with additional conjugation into one or two double bonds provided by ionone rings that terminate the carbon backbone on each end. Four methyl groups ($CH_3$) are at-

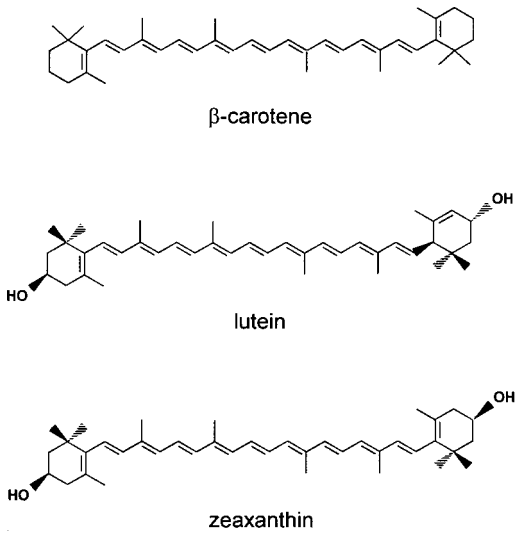


Fig. 1. Molecular structures of the carotenoid pigment species $\beta$-carotene, lutein, and zeaxanthin. All molecules feature a linear, chainlike conjugated-carbon backbone consisting of nine alternating carbon single (C—C) and double bonds (C=C) and four methyl groups attached as side groups. Structural differences between the molecules originate from the end groups attached to the carbon backbone. These end groups, termed ionone rings, contain an attached OH molecule in lutein and zeaxanthin, and they also differ in the location of an additional C=C bond in each ring. In lutein this leads to an effective conjugation length of 10 C=C bonds and in zeaxanthin to 11 C=C bonds.

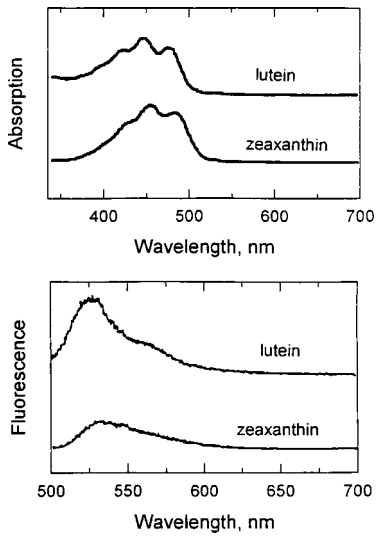


Fig. 2. Absorption (upper part) and luminescence spectra (lower part) of lutein and zeaxanthin solutions in THF. Solutions were optically thin (O.D. $\approx$ 0.3). Luminescence spectra were measured under 488-nm excitation.

tached to the backbone as side groups. Compared with $\beta$-carotene, lutein and zeaxanthin have an additional hydroxyl group (OH) attached to the 3 and 3′ positions of the ionone rings and therefore belong to the xanthophyll subfamily of carotenoids. Note that zeaxanthin differs from lutein in the location of one of the ionone ring double bonds, effectively providing a total of 11 conjugated double bonds compared with 10 for lutein.

The main optical properties of lutein and zeaxanthin, i.e., absorption and luminescence, are summarized in Fig. 2. Measuring solutions of the respective molecules dissolved in tetrahydrofuran (THF), we obtain in both cases strong electronic absorptions that occur in a broad band ($\sim$80-nm width) centered at $\sim$450 nm. The bands show clearly resolved vibronic substructure with a spacing of $\sim$1400 $cm^{-1}$ in both cases. Laser excitation of these carotenoids in the long-wavelength shoulder of their absorption bands leads in each case to a weak and spectrally broad luminescence with a small Stokes shift ($\sim$70 nm) between absorption- and emission-band peaks. Also, for lutein a vibronic substructure is again clearly visible in the luminescence, whereas for zeaxanthin the luminescence is structureless, thus indicating a stronger vibronic coupling. The most striking feature of the optical properties of these carotenoids is the fact that the luminescence signals are extremely weak, requiring a sensitive photomultiplier in combination with a photon counter for their detection. Comparing the signal strengths of the luminescence to organic dyes in the same experimental setup, we estimate the quantum efficiencies $\eta$ of the carotenoids to be of the order of $\eta \approx 10^{-5}$.

The observed optical properties of the carotenoids can be qualitatively understood within the concept of a configuration coordinate diagram, which is illustrated in Fig. 3. Shown here are the energies of the carotenoid molecule's three lowest electronic states as a function of a configuration coordinate. The configuration coordinate represents the displacement of a normal coordinate of the molecule's constituent atoms from its equilibrium position. In this picture, optical excitation of the molecule's conjugated $\pi$ electron leads in a fully allowed electric-dipole vibronic transition from the $1\,^1A_g$ singlet ground state to the $1\,^1B_u$ singlet excited state. Following excitation of the $1\,^1B_u$ state, the molecule relaxes very rapidly (within $\sim$200–250 fs in $\beta$-carotene[48]) via nonradiative transitions to the bottom of the $1\,^1B_u$ state. By analogy to the well-studied $\beta$-carotene molecule, two competing deactivation channels for the excited molecule can be assumed to occur from here: (a) radiative transition back to the $1\,^1A_g$ ground state and (b) nonradiative relaxation to another excited singlet state, $2\,^1A_g$, which is known to lie *below* the $1\,^1B_u$ state in polyenes. Obviously, the nonradiative deactivation channel (b) is very effective in the optical pumping cycle of the carotenoids, thus yielding only a very low luminescence quantum efficiency for channel (a). Furthermore, once in level $2\,^1A_g$, the electronic emission to the ground state is parity forbidden. The low $1\,^1B_u \rightarrow 1\,^1A_g$ luminescence efficiency ($10^{-5}$ to $10^{-4}$ in $\beta$-carotene[48]) and the absence of $2\,^1A_g \rightarrow 1\,^1A_g$ fluorescence result in extremely low luminescence signals for carotenoid molecules. This fact allows us to explore the resonant Raman scattering response of the molecular vibrations, which is usually orders of magnitude weaker than a fully electric dipole allowed and therefore potentially masks luminescence transition (see Fig. 2). Resonant Raman excitation is expected to excite the molecule from the lowest vibrational substate of the electronic ground state into higher vibrational substates of the $1\,^1B_u$ excited state. This is followed by rapid Stokes scattering transitions at fixed nuclear coordinates, i.e., downward in

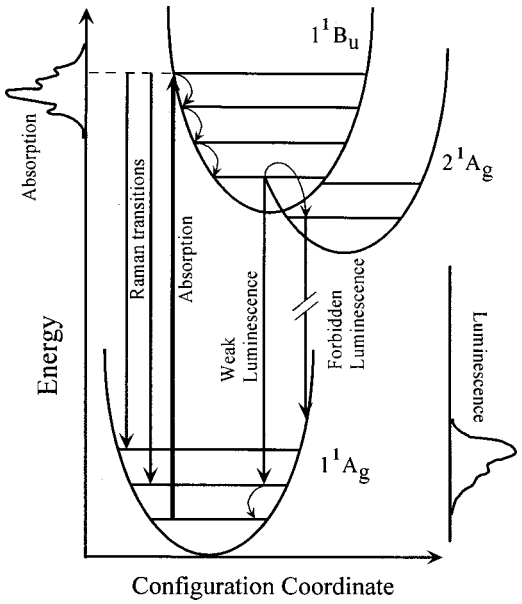


Fig. 3. Configuration-coordinate diagram for lowest energy levels of carotenoid molecules, with indicated optical excitation, nonradiative relaxation, luminescence, and Raman transition channels. Note that an even-parity excited state exists in these molecules ($2\,^1A_g$), which lies below the excited state reached after optical excitation ($1\,^1B_u$). Once an excited molecule has relaxed into this even-parity state after excitation, a luminescence transition to the even-parity ground state is parity forbidden. This feature allows one to observe resonant Raman transitions without spectrally overlapping luminescence.

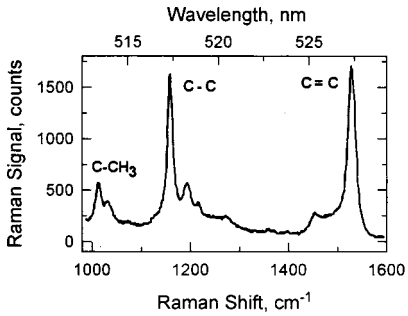


Fig. 4. Resonant Raman spectrum of a 7-$\mu$M solution of lutein in THF, showing three major Raman peaks at 1008, 1159, and 1525 $cm^{-1}$. The peaks correspond, respectively, to the rocking motions of the methyl components (C—$CH_3$) and the stretch vibrations of the carbon–carbon single bonds (C—C) and double bonds (C=C). The side peak at 1030 $cm^{-1}$ is an artifact and corresponds to THF. Laser excitation was at 488 nm.

the configuration coordinate diagram, into higher vibrational sublevels of the electronic ground state (see Fig. 3).

Indeed, we observe strong and clearly resolved Raman signals superimposed on a weak fluorescence background under resonant laser excitation, as shown in Fig. 4 for a 7-$\mu$mol solution of lutein in THF. For this measurement we placed the solution in a glass cuvette, excited it from the bottom with an argon laser, imaged the light excitation channel onto the entrance slit of a research-grade Raman spectrometer (Spex Triplemate), and measured the Raman spectrum unpolarized under standard 90-deg scattering geometry. The Raman response is characterized by two prominent Stokes lines at 1159 and 1525 $cm^{-1}$ (corresponding to wavelength shifts of 29.2 nm and 39.3 nm, respectively, for 488-nm excitation), with the 1525-$cm^{-1}$ line being the stronger one. These lines originate, respectively, from carbon–carbon single-bond (C—C) and double-bond (C=C) stretch vibrations of the conjugated backbone.[49] In addition, several weaker but clearly distinguishable Stokes signals appear at 1008, 1195, 1220, and 1450 $cm^{-1}$. The 1008-$cm^{-1}$ line is attributed to rocking motions of the molecule's methyl components.[49] We found that other carotenoids such as zeaxanthin, canthaxanthin, and astaxanthin had similar resonance Raman spectra in terms of Raman shifts and relative signal strengths.[43] An inspection of the scattering response over a larger spectral range revealed that the Raman signals were superimposed on a very weak fluorescence background originating from intrinsic carotenoid fluorescence that varied slightly in spectral shape and strength depending on the type of carotenoid molecule. In all cases the intensity ratio between Raman signal and background fluorescence was approximately 1:2 at the spectral position of the C=C vibration.

The Raman scattering intensity $I_s$ obtained for a molecular ensemble scales with the population density $N(E_i)$ of the molecules according to

$$I_s = N(E_i)\sigma_R(i \to f)I_L,$$

where the molecules are excited from level ($i$) to level ($f$); i.e., at fixed $N(E_i)$ it scales with laser intensity $I_L$, or at fixed laser intensity $I_L$ it scales linearly with $N(E_i)$. Here $\sigma_R$ is the Raman scattering cross section, given by[50,51]

$$\sigma_R(i \to f) = \frac{8\pi}{9\hbar\lambda_s^4} \times \left| \sum_j \frac{\langle \alpha_{ij}\rangle \mathbf{l}_L \langle \alpha_{jf}\rangle \mathbf{l}_s}{\omega_{ij} - \omega_L - i\Gamma_j} + \frac{\langle \alpha_{ji}\rangle \mathbf{l}_L \langle \alpha_{jf}\rangle \mathbf{l}_s}{\omega_{jf} - \omega_L - i\Gamma_j} \right|^2,$$

where $\langle \alpha_{ij}\rangle$ is the expectation value of the component $\alpha_{ij}$ of the polarizability tensor; $\mathbf{l}_L$, $\mathbf{l}_S$ are the polarization unit vectors of incident and scattered light, respectively; and $\Gamma_j$ is the homogeneous width of molecular level $j$.

For any chosen excitation and collection geometry, the scattering cross section is a fixed value. In optically thin samples, the population density $N(E_i)$ is proportional to the ground-state concentration of the molecules, and in this case the Raman scattering intensity scales linearly with concentration of the molecules.

## 3. RAMAN MEASUREMENTS OF EXCISED RETINAL TISSUE

To apply Raman spectroscopy to the measurement of macular pigments in the human eye, we investigated first a 180-deg backscattering geometry. Furthermore, we established whether carotenoid Raman signals with sufficient signal-to-noise ratios can be obtained from thin, film-like retinal tissue and whether the Raman spectra are free of any potentially interfering background signals. The latter may originate from other ocular tissues in the path of the Raman excitation beam or from molecules such as rhodopsin or retinoids, which are present in the retina in high concentrations.

To investigate the Raman excitation wavelengths that are useful for excitation of retinal tissue, we show in Fig. 5 the absorption spectrum of a typical excised flat-mounted human retina. For this we removed the retinal pigment epithelium from a 5-mm-diameter macular tissue punch, mounted the sample between two glass cover slips, and measured the absorption with a conventional absorption spectrometer which employs a measuring beam of ~2-mm diameter. The macular pigments are clearly visible because of their characteristic absorption band in the 450-nm range, and they also display the vi-

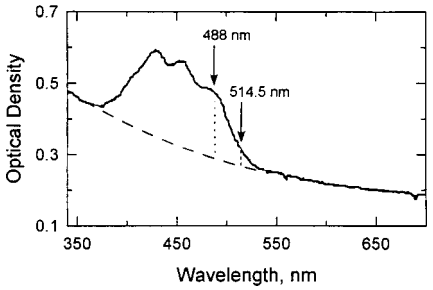


Fig. 5. Absorption spectrum of an excised, flat-mounted human retina in the near-UV–visible wavelength region, revealing typical absorption characteristics of carotenoid pigments near 450 nm (the retinal pigment epithelium of the retina was removed for this measurement). Note the remarkable similarity of the absorption of the biological tissue to the absorption of the carotenoid solution in Fig. 2. Dashed curve, Rayleigh scattering background; the arrows, wavelength positions of the 488- and 514.5-nm argon laser lines that are useful for resonant Raman excitation.

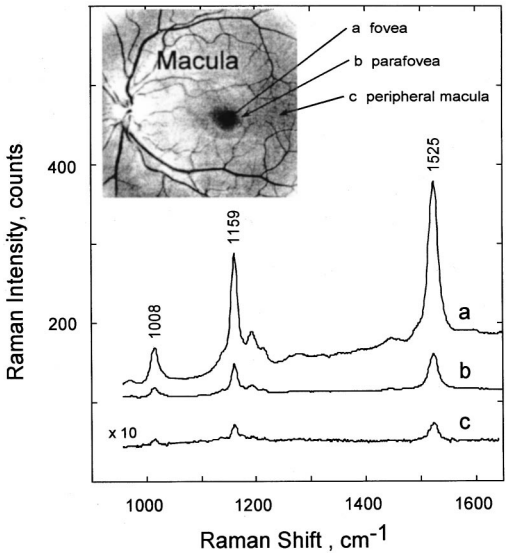


Fig. 6. Resonance Raman spectra of a flat-mounted human retina. Spectra were observed under excitation with 488-nm argon laser light in the center (trace a), 0.5 mm away from the center (trace b), and at the periphery (trace c) of the macula. The intensity scale of trace c is expanded by a factor of 10 for clarity. Illumination conditions: 488-nm, 40-mW, 300-$\mu$m spot size, 9 s collection time. Spectra were recorded in backscattering geometry.

bronic substructure characteristic for lutein and zeaxanthin. The absolute optical density in the peak of the absorption band is ~0.3 for this particular retina, taking into account (i.e., subtracting) the smoothly varying Rayleigh scattering component under the curve. It is evident from this absorption behavior that efficient resonant Raman excitation is achievable with the 488-nm argon laser line that overlaps the absorption band in the spectral range of the $0 \rightarrow 1$ vibronic transition of the carotenoid molecules. In comparison, the absorption measurements show that excitation with the 514.5-nm argon laser line would excite the carotenoids in the long-wavelength shoulder at ~20% band peak height.

On the basis of these measurements, we tested as excitation sources the vertically polarized 488- and 514.5-nm lines of an argon laser, and we tested the Raman response from flat-mounted retinas and from human eyecups in a 180-deg backscattering geometry. For this, we reduced the laser power to several milliwatts with a neutral density filter and eliminated the laser plasma lines with a spectral filter consisting of a combination of a 600-lines/mm grating and a slit. The laser was directed through a beam splitter and weakly focused onto a sample with a 10-cm focal length lens. The backscattered light was imaged onto the entrance slit of a Raman spectrometer with the beam splitter and an additional lens. The Raman spectrometer employed two stray-light rejection gratings with 300 lines/mm, a dispersion grating with 1200 lines/mm, and a liquid-nitrogen-cooled silicon CCD detector array with 25-$\mu$m pixel width.

The Raman spectra obtained with this spectrometer for an excised flat-mounted human retina are shown in Fig. 6. Raman carotenoid peaks at ~1159 and 1525 $cm^{-1}$ are obtained with good signal-to-noise ratio when the laser excitation beam is aimed at the foveal and parafoveal areas (traces a and b), and they decrease by at least a factor of 30 as the beam is moved toward the peripheral retina (trace c). This behavior correlates well with the known distribution of carotenoids in the human retina as determined by high-performance liquid chromatography (HPLC) or psychophysically.[2,19]

Note that the Raman spectra are obtained with excellent signal-to-noise ratio and that they are free of any interfering background fluorescence or Raman signals from other molecules besides carotenoids. Subsequent experiments on eyecup preparations with intact vitreous and retinal pigment epithelium confirmed that other ocular tissues also have insignificant fluorescence and resonant Raman signals in the spectral region of interest.

## 4. RAMAN INSTRUMENT FOR CLINICAL APPLICATIONS

In our initial measurements we used a research-grade, complex and bulky Raman instrument (Spex Industries). This instrument is designed for high-wavelength flexibility and high spectral resolution but not for high light throughput. As a consequence it requires excessively high laser power levels for the collection of Raman spectra having acceptable signal-to-noise ratios. It is therefore not useful for our goal of ultimately detecting carotenoid pigments in the retina of living humans. Instead, this application requires that the ocular light exposure[52] during a measurement be limited to prevent both photochemically and thermally induced retinal injury, as specified by American National Standards Institute (ANSI) safety regulations (see below). Furthermore, for an instrument to be useful in a clinical setting, it needs to be compact and portable. To meet all these requirements we constructed a compact, portable, fiber-based, and computer-interfaced Raman instrument. The layout is shown schematically in Fig. 7. The instrument sacrifices unneeded spectral resolution for the benefit of increased light throughput. Also, it can be interfaced to a fundus

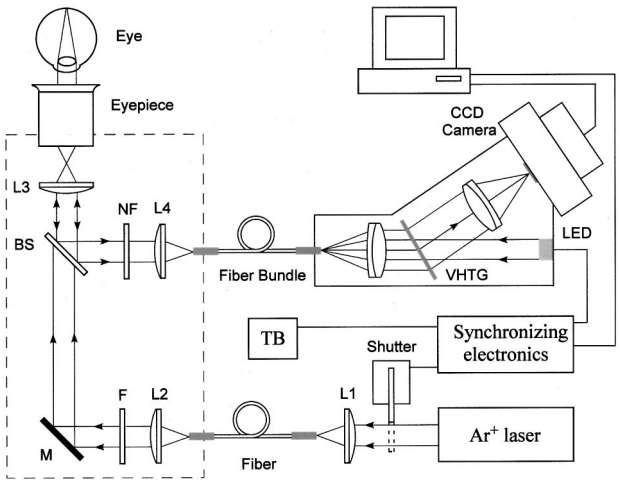


Fig. 7. Schematics of the fiber-based, portable Raman instrument for clinical applications. The instrument consists of an argon laser (lower right) for excitation, a light-delivery and collection module, a spectrograph (upper right) and electronics. The subject looks into the light module through an eyepiece and aligns his/her head position before a measurement. See text.

camera to help monitor the delivery of the excitation laser beam to the foveal area of the retina in living eyes.

An important component of our device is the beam delivery and collection optics module shown in the lower-left part of Fig. 7. The excitation laser beam originates from a small air-cooled argon laser operating on the 488-nm line. It is routed via optical fiber into the module, collimated by lens $L_2$, transmitted through filter F, and reflected by mirror M; it then passes through dichroic beam splitter BS, and is finally imaged onto the macula by a combination of an auxiliary lens, $L_3$, and an eyepiece. The laser-excitation fiber is a multimode fiber with a core diameter of 500 $\mu$m and a numerical aperture N.A. = 0.22. The dielectric bandpass filter, F, which is placed in the excitation path, blocks any spectral components outside a narrow 3-nm bandwidth centered around the 488-nm excitation wavelength. This blocking effectively suppresses fiber fluorescence and laser plasma lines in the Raman-scattering spectral range of interest. The Raman-scattered, wavelength-shifted light is collected in 180-deg backscattering geometry with the same eyepiece–lens combination used to deliver the excitation beam and is reflected by the dichroic beam splitter, BS, into a separate light-collection path. A holographic rejection notch filter, NF, which effectively blocks the Rayleigh-light components of the scattered light occurring at the excitation wavelength, is placed in this path before coupling of the Raman-scattered light into a collection fiber with lens $L_4$. The holographic rejection notch filter NF suppresses the excitation light by six orders of magnitude while transmitting the Raman-shifted light components with 80% efficiency. The light-collection fiber is a fiber bundle consisting of 96 individual multimode fibers, each with 70-$\mu$m core diameter, and higher than 55% overall transmission owing to a high fiber filling factor. The input cross section of the fiber bundle is circular (1-mm diameter), and the output cross section is rectangular (100 $\mu$m $\times$ 8.6 mm), to match the rectangular input slit geometry of a home-made spectrograph designed for high light throughput.

This spectrograph employs two achromatic lenses for light collimation and a volume holographic transmission grating (VHTG) glued onto the surface of a 45-deg prism. The prism (not shown in Fig. 7) is used to compensate for aberrations introduced by the collimating-lens–VHTG combination. The line density of the VHTG is 1200 $mm^{-1}$, and the diffraction efficiency is ~80% for nonpolarized light. The *f*-number of the spectrograph is 2 and thus is ideally matched to the *f*-number of the individual multimode fibers comprising the fiber bundle.

The dispersed spectrum is imaged onto the 8.63-mm $\times$ 6.53-mm silicon chip (Texas Instruments, model TC-241) of a CCD camera (Santa Barbara, Inc., model ST6v). The CCD chip consists of an array of 750 by 121 pixels each having an area 11.5 $\mu$m $\times$ 27 $\mu$m. It has a relatively low detector noise with a combined dark and read-out noise smaller than ~8 counts. The quantum efficiency of this chip in the blue–green spectral range of interest is ~55%. We chose to vertically bin pixels oriented perpendicular to the dispersion plane of the spectrograph into "super pixels" and thus achieved simultaneously a low read-out noise (24 counts per super pixel) and a high read-out speed (~0.5 s). The resolution limit of the instrument is 20 $cm^{-1}$.

Our instrument features several provisions to aid optical alignment of the instrument to the human eye. An optical shutter is designed such that even in the closed state it transmits a very small portion of the blue argon laser light used for Raman excitation. This way, a subject looking into the instrument sees a blue spot originating from the end face of the excitation-light delivery fiber. Using a proper choice of focal lengths for lenses $L_2$, $L_3$, and the eyepiece, we realized a 1:2 magnification, effectively imaging the excitation fiber end face into a 1-mm-diameter spot on the retina. Furthermore, using a low-power light-emitting diode, LED, we generated an additional red polka-dot pattern, originating from the facets of the light-collection fiber bundle as an alignment aid for the subject. With the focal length of lens $L_4$ chosen to be twice that of lens $L_2$, the 1-mm circular face of the red-illuminated fiber bundle is imaged at the patient's retina as a 1-mm spot and thus has the same diameter as the blue-illuminated retinal excitation spot. Before a measurement, a subject overlaps the blue disk and the red polka-dot pattern to ensure proper alignment of his or her eye with respect to the instrument. The subject achieves this alignment simply by appropriate positioning of the head. An adjustable focus allows the subject to correct for refractive error if needed. Alternatively, the subject can simply wear his or her usual glasses or contact lenses. After the subject has signaled alignment, the instrument operator pushes a trigger button, TB. The synchronized electronics momentarily turns off the red LED aiming beam (to avoid exposure of the CCD detector), opens the shutter to allow laser-light projection onto the retina, and triggers the data acquisition. After a preset measurement time period of 0.5 s, the instrument closes the laser shutter, digitizes the backscattered light, downloads data into computer memory, and initiates software processing for spectral display, as described in more detail below. The instrument is interfaced to a small personal computer with home-developed Windows-based software for data acquisition and processing. All postexposure processing takes only ~0.5 s, and thus the instrument realizes near-real-time display of the final Raman spectrum and other operating parameters on the computer monitor after each measurement. Using the Windows-based computer interface, the software facilitates a number of other functions: It permits the operator to properly initiate the hardware, and it checks all necessary communications between the computer and the CCD camera. It automatically measures the dark spectrum and subtracts it whenever a measurement is made, processes the spectra, saves the data as text ASCII files, and, finally, helps the operator to properly shut down the instrument.

To comply with ANSI safety regulations, the ocular exposure levels used in our Raman instrument have to stay below certain specified threshold levels. According to the latest issue, ANSI Z136.1-2000,[53] ocular exposure levels have to be limited to protect the eye both from photochemically and thermally induced retinal injury under our measurement conditions (visible light near 0.5 $\mu$m, immobilized eyes, exposure time of 0.5 s). The photochemical limit for retinal injury (Sec. 8.3.1 of the ANSI

guidelines) is listed as 2.7 $C_B$ J/cm$^2$, where $C_B$ is a wavelength correction factor, and results in 15.5 J/cm$^2$ with $C_B = 5.75$ for 488 nm. The thermal limit for retinal injury (Sec. 8.3.2), valid for an exposure time $0.07 < t < 0.7$ s, has to be calculated from the laser spot present at the cornea and is listed as $1.8(\alpha/1.5)t^{0.75}$ mJ/cm$^2$. Here $\alpha$ is the angle of the laser source at the laser source at the location of the viewer, measured in milliradians. Using $t = 0.007\,s$ and $\alpha = 58.8 \times 10^{-3}$ rad, we obtain an energy density of 9.6 mJ/cm$^2$ at the cornea for the thermal-exposure limit of the retina.

In a typical single-exposure measurement with our instrument (0.5-s ocular exposure with 0.5-mW light at 488 nm), a total laser energy of 0.25 mJ is projected onto an 8-mm-diameter spot at the cornea and a 1-mm-diameter spot on the retina. This corresponds to a retinal exposure level of 32 mJ/cm$^2$, which is ~480 times lower than the 15.5-J/cm$^2$ photochemical limit. For the ocular exposure used, we calculate a level of 0.5 mJ/cm$^2$ considering that the light energy of 0.25 mJ is distributed over a spot-size diameter of 8 mm at the cornea; therefore this exposure level is ~19 times below the thermal limit of 9.6 mJ/cm$^2$ for retinal injury.

The appearance of the computer monitor after a typical measurement is shown in Fig. 8. On the left side of the screen a "safety/dosimetry control" table is displayed. This table shows the exposure dose as a function of the chosen excitation laser power, exposure time, and area of the excitation spot on the retina. It also contains the ratio of the light dose with respect to the maximum permissible exposure dose. As can be seen from the table, under the typical experimental conditions (exposure time 0.5 s, laser power 0.5 mW, spot size 1 mm), a safety factor of ~19 is realized.

The central part of the screen shows the measured Raman spectrum superimposed on a spectrally broad background spectrum caused by fluorescence of the retina. This spectrum is a difference spectrum resulting from the subtraction of a dark spectrum (recorded before a measurement) from the measured spectrum. The observer may view this spectrum to obtain general spectral information, i.e., shape and height of the combined

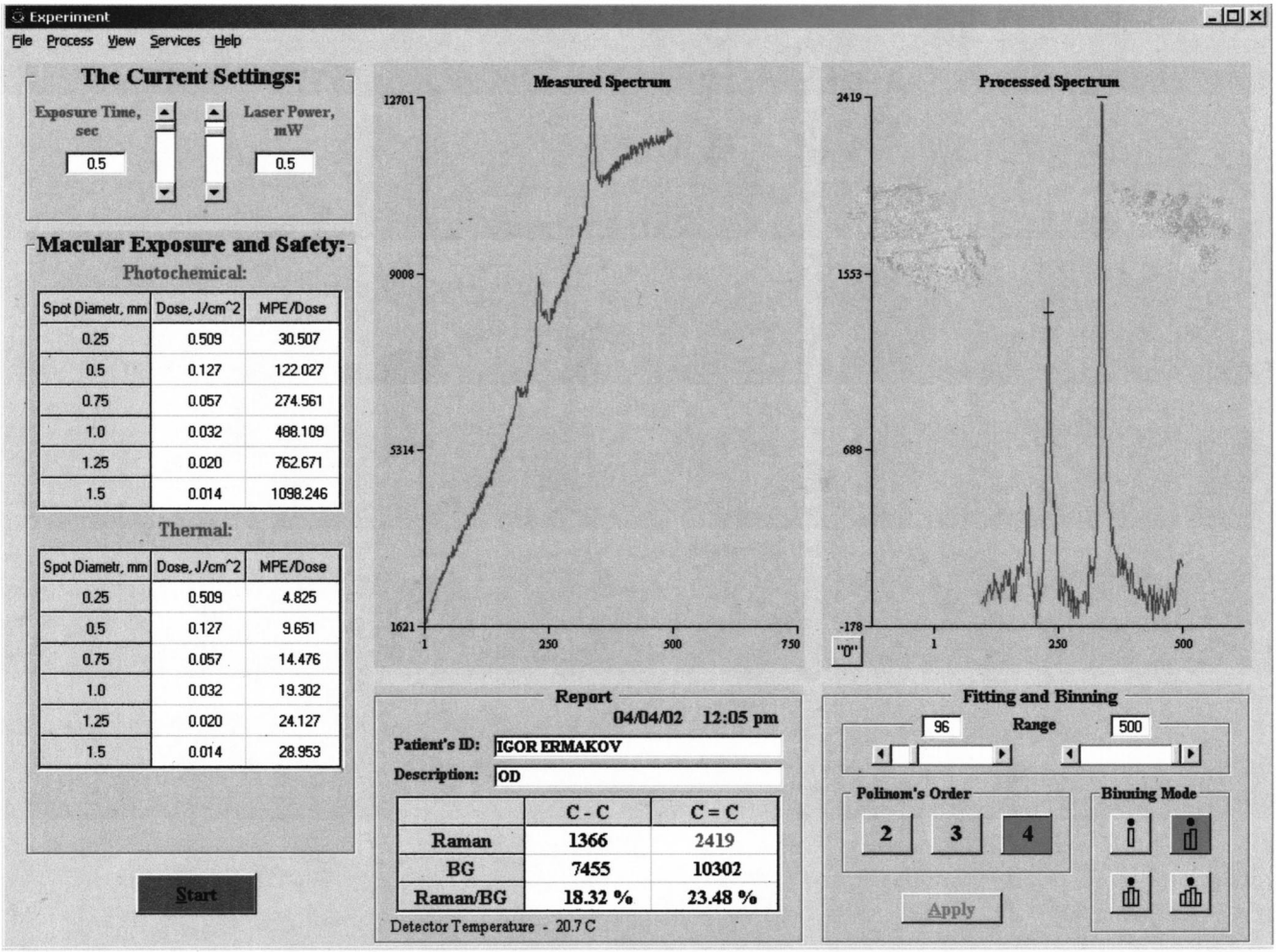


Fig. 8. Display of a typical Raman measurement on the computer monitor. The spectral displays (center and center right) consist of plots of signal intensity (counts) versus pixel number of the CCD camera array. The spectrum in the center shows the unprocessed spectrum of a measurement and includes fluorescence background as well as superimposed Raman peaks. The spectrum on the right shows the Raman spectrum after polynomial fit of the fluorescent background and subtraction of that background. The window at center bottom shows the Raman peak heights of the C—C single-bond and C═C double-bond vibration, the magnitudes of the background signals, and the ratios of Raman to background signals at corresponding pixels.

fluorescence/Raman spectra. The right part of the screen displays the measured carotenoid Raman spectrum after subtraction of the overlapping fluorescence background, which is accomplished by polynomial fitting of the background spectrum and subsequent subtraction from the spectrum displayed in the central window. To derive the shape of the background, we use all data points in the selected wavelength range except those in the vicinity of the Raman peaks. All these data points are curve fitted to a user-selected polynomial of up to fourth order, and the computed polynomial curve is subtracted from the original spectrum. This results in a curve containing spectral information exclusively from the Raman response of the macular carotenoids. To obtain an accurate reading of the Raman peak heights, we eliminated the influence of potentially overlapping noise spikes in the spectrum by fitting the measured Raman line shapes with Lorentzians in a single-parameter fit, where we used the known wavelength positions and (instrumentation-broadened) spectral widths of the Raman peaks of interest. The calculated values for the intensities of the C—C single-bond and C═C double-bond peaks, along with the values for the fluorescence intensity under those peaks and the ratios of the Raman intensities to the background, are tabulated in a "Report" window (see lower-middle part of Fig. 8). In addition, this window allows one to input the subject's personal data, contains a date/time stamp, and saves this information along with the spectra.

It is possible to improve the quality of the spectrum, i.e., the signal-to-noise ratio, by summing up to four neighboring pixels in a "binning-mode" option (lower-right part of Fig. 8). Furthermore, signal-height indicator markers for the Raman peaks and the baseline can be used to evaluate the quality of the data processing.

For a typical carotenoid Raman measurement, we displayed the spectrum on the computer screen, identified the sharp carotenoid Raman peaks riding on the broad fluorescence background, fitted the broad background with a fourth-order polynomial, and subtracted this background from the measured spectrum. As a measure of carotenoid concentration, we chose the final peak height of the C═C double bond signal at 1525 $cm^{-1}$.

To find a correlation of the Raman readings with the actual carotenoid concentration of the living retina, we conducted several initial calibration Raman experiments using filmlike samples of carotenoids on artificial maculae consisting of thin polyvinylidene difluoride (PVDF) substrates. Furthermore, we used an anatomically correct model eye to test the Raman detection of these samples when they were attached to the macula location of the model eye.

The PVDF samples were spotted with various solutions of known carotenoid concentrations, thus providing dried, ~3-mm diameter spots with lutein concentrations corresponding to average carotenoid concentrations typically found in excised human macular samples, as measured by HPLC. We observed strong and clearly resolved carotenoid Raman signals at 1159 and 1525 $cm^{-1}$, superimposed on a weak fluorescence background under resonant laser excitation, with a spectral response essentially identical to the Raman spectra obtained for lutein in solution except for a slightly larger fluorescence background.

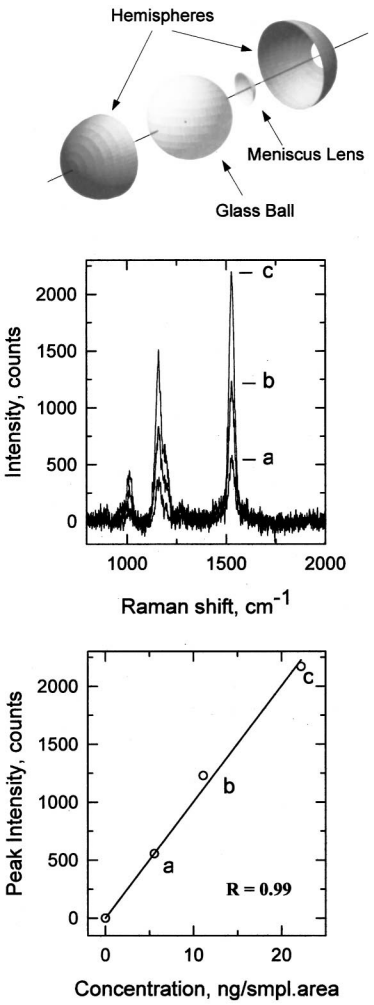


Fig. 9. Raman scattering of lutein PVDF samples attached to the "macula" of a model eye. Upper part, schematic of the model eye, which consists of two hemispheres with internal meniscus lens and glass ball. Middle part, Raman spectra in the carotenoid-stretching vibration range for three increasing concentrations: 5.5 (a), 11 (b), and 22 (c) ng/sampled area. Bottom part, Raman signal of C═C double bond peak versus concentration, showing linear dependence with near-unity correlation coefficient.

This test demonstrates that strong, well-resolved Raman signals can be readily obtained with excellent signal-to-noise ratios even for thin, filmlike samples with use of eye-safe low laser-power levels. Furthermore it shows that a 180-deg backscattering geometry, as required for Raman measurements of intact human and laboratory primate eyes, poses no inherent problems.

Next we measured the Raman response from similar artificial maculae with differing lutein concentrations attached to the "macula location" of a model eye (Nidek, Inc., Japan). The model (see Fig. 9) consisted of a hollow plastic sphere the same size as a typical human eye and featured a plastic double meniscus lens. The inside of the plastic sphere contained a glass ball. The effective focal length of the model eye was 2 cm and thus simulated the combined refractive powers of human cornea, eye lens, and vitreous humor. We measured the Raman spectra for three artificial maculae, testing humanlike carotenoid concentrations of 50-, 100-, and 200-ng lutein per

3-mm-diameter spot. For each "macula," the Raman instrument measured an effective 1-mm-diameter spot. Therefore the measured Raman signals corresponded to 5.5-, 11-, and 22-ng carotenoids per macula. The results are shown in Fig. 9 and demonstrate a linear relationship between carotenoid Raman peak height (intensity) and carotenoid concentration. The coefficient of linear correlation, $R$, is close to 1 ($R = 0.99$) in these measurements. These tests demonstrate that excellent linear tracking of carotenoid concentration is possible with our instrument.

In another experiment we compared the Raman spectra of an artificial macula placed on a glass coverslip with the spectra obtained when the macula was placed on a black paper substrate. In both cases the ratio of the Raman signal to the fluorescence background was found to be ~1:2. This shows that the predominant Raman response originates from backscattering and that small reflections as expected from a glass–air interface or a black strongly absorbing object simulating the retinal pigment epithelium have a negligible influence on the Raman data.

## 5. RAMAN MEASUREMENTS OF THE LIVING PRIMATE RETINA

In the next step, we tested the Raman detection of carotenoids in the living eyes of primates. A total of eight monkeys were used under an institutionally approved animal-use protocol. For these experiments we interfaced our Raman instrument with a fundus camera, as shown schematically in Fig. 10. In addition to the argon laser used for Raman excitation, we routed a He–Ne laser through the light-delivering fiber, using appropriate coupling optics and a dichroic beam splitter, BS 3. The He–Ne laser is colinear with the Raman laser and of identical spot size, serving as a pilot beam that is visible to the observer viewing the retina of the subject eye through the fundus camera. It precisely targets the spot on the retina that is exposed to the Raman (argon) excitation laser during a measurement. Also, since the nerve head of the primate retina is known to have a typical diameter of ~1 mm, the relative size of the pilot beam's spot size (and hence the identical spot size of the argon laser) can be estimated by simply comparing it with the optic nerve head, as shown in Fig. 11.

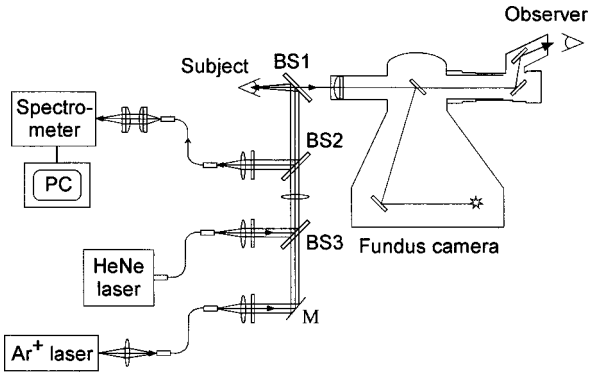


Fig. 10. Experimental setup for Raman measurements of primate retinas. An instrument similar to that shown in Fig. 7 is interfaced to a fundus camera to permit viewing of the animal's retina while targeting the macula with a pilot laser beam before a measurement.

To accurately target the Raman measurements on the retina, we attached a video camera to the eyepiece of the fundus camera and observed the pilot beam on a monitor while taking successive Raman readings. The pilot laser spot could be seen clearly on the monitor while being positioned onto the target area (macula) of the primates. Figure 11 shows the relative positions and sizes of the beams with respect to the physiological features of the retina, along with the corresponding Raman spectra. All three characteristic carotenoid Raman peaks are clearly distinguishable with an acceptable signal-to-noise ratio provided that the argon laser is targeted onto the fovea (bottom-right panel). As expected, nonfoveal areas of the macula, where the carotenoid concentration is ~10-fold lower, show only very weak carotenoid Raman peaks (see top-right panel). Peripheral retinal areas, where the carotenoid concentration is approximately 100-fold lower, showed only background fluorescence and no discernable carotenoid Raman peaks (data not shown).

In the experiment whose results are plotted in Fig. 12, we tested our resonance Raman system on six intact monkey eyes harvested from four monkeys in one measurement session under identical conditions. After completion of the Raman carotenoid measurements, the enucleated eyes were dissected and the lutein and zeaxanthin levels in the macula (5-mm circular punches) were measured by HPLC. Although there is a linear correlation between the two measurement techniques, the correlation is not nearly as strong as in our previously published data on flat-mounted human cadaver maculae.[43] We attribute the greater variability of the *in vivo* experiments to two factors. First, the monkey macular punches were substantially larger than the area illuminated by the argon laser (5-mm diameter versus 1-mm diameter) since it is difficult to dissect extremely small pieces of retinal tissue with accuracy. Although the majority of the macular carotenoids are present in the central millimeter of the macula, the ~25-fold differences in measurement areas could introduce substantial variability when the two methods are compared. Second, we found it quite challenging to align the fovea of anesthetized monkeys for Raman measurements. Fortunately, this second problem is less of an issue in our clinical Raman instrument, since living humans will generally fixate voluntarily on an aiming beam (unless they have lost central fixation as a result of severe ocular pathology), which greatly simplifies the foveal alignment.

## 6. RAMAN MEASUREMENTS OF THE LIVING HUMAN RETINA

### A. Methods

#### 1. Subjects

Adult subjects were recruited from the clinic population of the Moran Eye Center of the University of Utah. All subjects gave informed consent by signing a form approved by the Human Subjects Review Board. All normal subjects were examined ophthalmoscopically after maximal pupillary dilation with 0.5% proparacaine, 2.5% phenylephrine, and 1% tropicamide eye drops[54] to confirm that they were free of macular pathology or visually significant

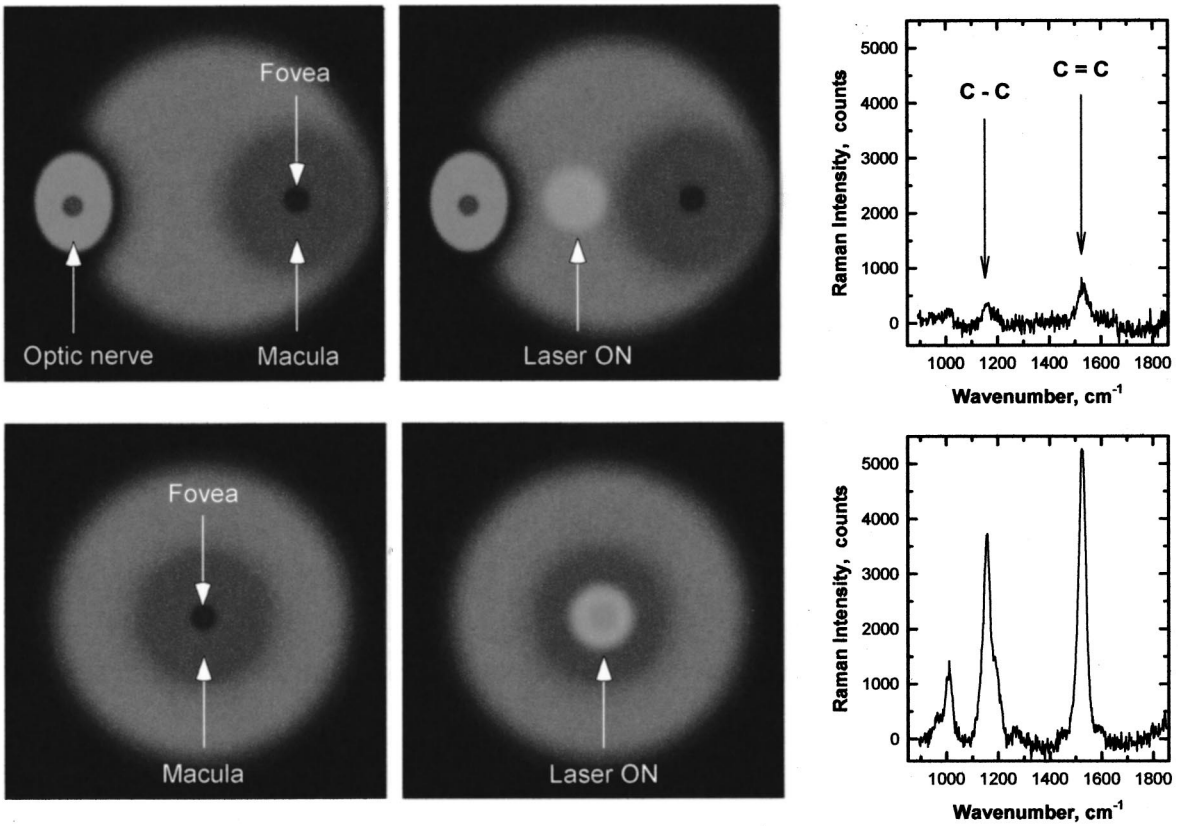


Fig. 11. Views of illuminated primate retinas (four images) showing physiological structures, along with associated fluorescence-background-subtracted Raman spectra (right). Top two images, views when the laser is turned off (left) and when the laser is illuminating the retina between the optic nerve and the fovea (right). Bottom two images, corresponding views when the fovea is targeted. See text.

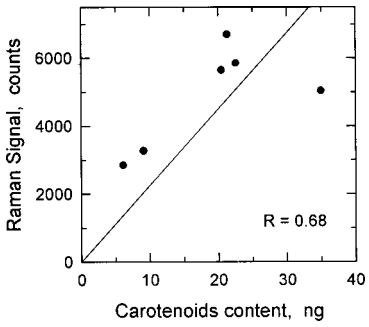


Fig. 12. Correlation of Raman signals, obtained for the C=C double-bond vibration at 1525 $cm^{-1}$, with the carotenoid content of six monkey maculae as determined by HPLC. A linear fit to the data results in a correlation coefficient of 0.68.

cataracts. Subjects with dilated pupil size of less than 6 mm were not enrolled. The average dilated pupil size of all of the enrolled subjects was 8 ± 1 mm [mean ± standard deviation (S.D.)] as measured by a pupil gauge on a near-card or on a slit-lamp, and there was no trend of change of dilated pupil size with age ($P = 0.342$ by one-way analysis of variance), a finding consistent with a recent report that dilated pupil size is determined predominantly by heredity rather than by age.[55] Subjects with intraocular lenses placed after surgical cataract removal were included. Intraocular pressures were checked by Tonopen, because Goldmann applanation tonometery with fluorescein drops led to very large fluorescence artifacts that interfered with macular pigment measurements for many hours.

*2. Measurement Protocol*

Subjects were brought into a darkened room and asked to fixate on the polka-dot array of red dots (the collection fibers illuminated with a red light-emitting diode) while resting the forehead against the device. They were then asked to adjust the head position to superimpose a similar-sized blue–green pilot laser beam spot over the array of red dots. Subjects with significant refractive error wore their usual glasses or contact lenses. When the subject was ready, the fovea was illuminated with 500-$\mu$W, 488-nm argon laser light for 0.5 s. The spot size at the retina was 1 mm (3.5 deg) as measured by direct observation through the fundus camera and by measurement of the afterimage on an Amsler grid. Five measurements were made on each eye at intervals of 30–60 s to allow the flash afterimage to fade. Since subjects occasionally blink or misalign, the mean and standard deviation of the three best out of five measurements were used for data analysis.

## B. Results and Discussion

*1. Sensitivity*

Typical Raman spectra from the macula of a healthy volunteer, measured with dilated pupil (diameter ~8 mm) in a single exposure, are shown in Fig. 13 and clearly reveal

carotenoid Raman signals superimposed on a weak and spectrally broad fluorescence background. The upper trace corresponds to the spectrum as measured and the bottom trace to the same spectrum after subtraction of the fluorescence background, shown on an expanded scale. The carotenoid level in the volunteer's eye is indicated by the strength of the carbon double-bond signal and amounts to 1700 counts. Using the model-eye calibration standard described above (Fig. 9), this would amount to ~16-ng carotenoid concentration in the volunteer's fovea, which is a reasonable value for a human. Extrapolating from Fig. 13, we expect our instrument to be able to measure at least a factor-of-15-lower carotenoid concentrations.

The ratio between the C=C Raman signal and the background fluorescence is ~1:3, which is close to the ratio of the carotenoid response in solution (see Section 2) and shows that in the wavelength region of interest there is only little contribution to the background signal from molecules other than carotenoids.

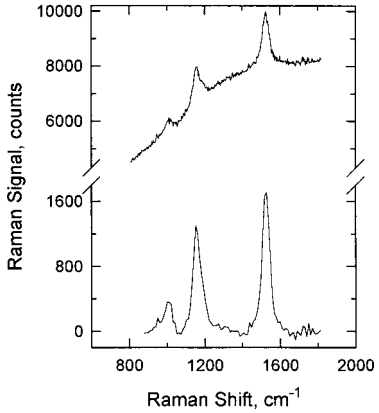


Fig. 13. Raman spectra of a healthy human volunteer, measured with dilated pupil. Top trace, before background subtraction; bottom trace, after subtraction of fluorescence background. Excitation 488 nm, 0.5 s, 0.5 mW, 1-mm spot size on retina.

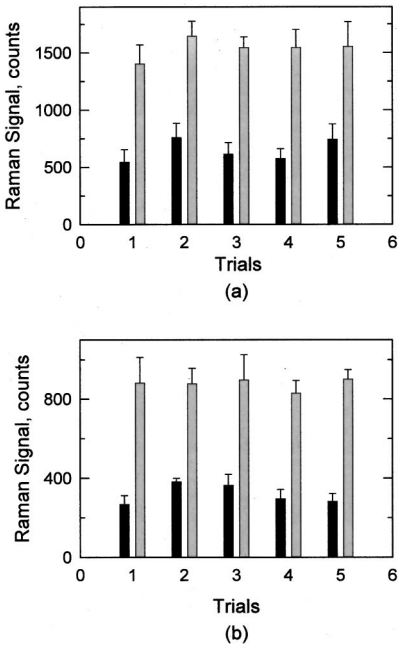


Fig. 14. Repeatability of Raman measurement of macular pigments measured in two subjects, ages 26 (a) and 37 (b). Raman intensities are shown for dilated (gray bars) and undilated (black bars) pupils in each case, and measured over a two-week period in five sessions (represented by the five pairs of bars). Mean ±S.D. of 5–7 measurements for each session is shown.

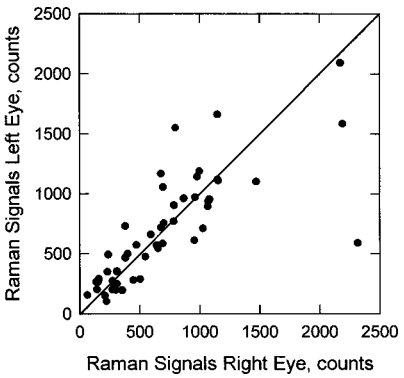


Fig. 15. Raman signals for left and right eyes of normal subjects, revealing symmetry of macular pigment concentrations in both eyes.

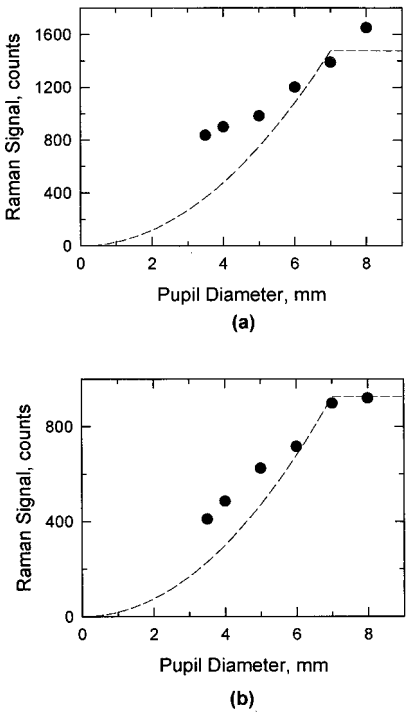


Fig. 16. Variation of the Raman signal with pupil diameter for two subjects (circles), showing approximately twofold increase of the Raman signal after full pupil dilation. Above ~7-mm pupil diameter, signals stay constant. Dashed curve, theoretically expected variation of the signal with pupil diameter.

*2. Reproducibility*

In the experiment whose results are shown in Fig. 14, two subjects [ages 26 (a) and 37 (b)] repeated their macular pigment measurements in five consecutive sessions over a two-week period before and after pupil dilation. Typical standard deviations from five measurements were smaller than ±15%, and the intersession reproducibility was high. Macular pigment levels correlated well between right and left eyes in normal subjects age 21–84, as shown in Fig. 15.

*3. Signal versus Pupil Diameter*

The same two subjects had multiple measurements performed while their pupils were dilated pharmacologically. Between measurements the pupil diameters were measured in ambient light. As shown in Fig. 16, carotenoid Raman signals (circles) gradually increase as the pupils slowly dilate to their maximum diameter, leveling off at ~7-mm diameter. In the fully dilated state, the signals are typically twice as large as in the undilated state. The dependence of the system Raman response on pupil diameter $D$ can be understood by considering the geometrical light throughput of the instrument, $F_{\text{inst}}$, which is designed with an effective aperture of 7 mm (defined by the magnified aperture of the light-collection fiber bundle), and the light throughput of the eye, $F_{\text{eye}}$, which scales quadratically with pupil diameter. Both result in the overall throughput of the system, $F_{\text{syst}} = \min\{F_{\text{inst}}, F_{\text{eye}}\}$, which is indicated in Fig. 16 by the dashed curves for the two measurements. The instrument aperture limits the overall light throughput to $F_{\text{syst}} = F_{\text{inst}}$ for $D \geqslant 7$ mm. The light throughput of the eye is given by $F_{\text{eye}} = kD^2$, where $k$ is a constant accounting for the transmission properties of the average human eye. The total light throughput of the system is thus controlled by the pupil diameter for the case $D < 7$ mm, and it is limited by $F_{\text{instr}}$ when $D$ exceeds 7-mm diameter.

The data in Fig. 16 reveal that measured signal levels are noticeably higher than expected levels for pupil diameters below ~6 mm. This effect appears because the incompletely dilated pupil still changes its diameter while measured: When initially exposed to the bright measuring beam, the eye reflex contracts the pupil from a dark-adapted large diameter to a smaller diameter determined by the counteracting effects of light intensity and progressing pharmacological immobilization. Since light exposure and pupil reaction time are comparable (~0.5 s), the effective pupil diameter is higher than the diameter measured under ambient light conditions (which is shown as the abscissa in Fig. 16). As a consequence of these pupil diameter effects for clinical instrumentation trials, we chose to measure only fully dilated (8-mm mean ±1 mm S.D.), immobilized eyes of subjects, thus ensuring maximized light throughput as well as defined measuring conditions under bright-light exposure.

*4. Signal versus Age*

A total of 212 eyes of 140 normal subjects aged 21–84 and free of macular pathology or visually significant cataracts were measured using the Raman instrument; the results are shown in Fig. 17. Approximately one half of the subjects (72) had biocular measurements. There is a striking decline of the Raman signal with increasing age. This finding is in marked contrast to a recent psychophysical study that found a slight increase of macular pigment with increasing age[25] but correlates well with two other psychophysical studies that also noted a decline with age.[23,26] Pupil size could not be the source of the decline since all subjects were fully dilated pharmacologically, and subjects who could not dilate to at least 6 mm were excluded. Mean ± S.D. pupil size was 8 ± 1 mm in both younger and older individuals, as shown in Fig. 18.

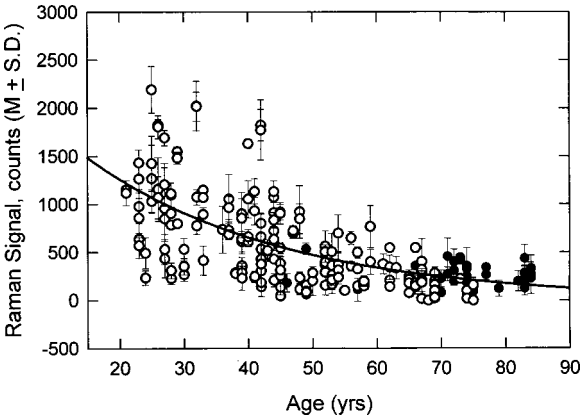


Fig. 17. Raman macular pigment measurement of 212 normal eyes as a function of subject age, revealing statistically significant decrease of macular pigment concentration with age. Solid circles represent subjects with clear prosthetic intraocular lenses. Mean ±S.D. of the best three out of five measurements are shown. Data are not corrected for decrease of ocular transmission with age. See text.

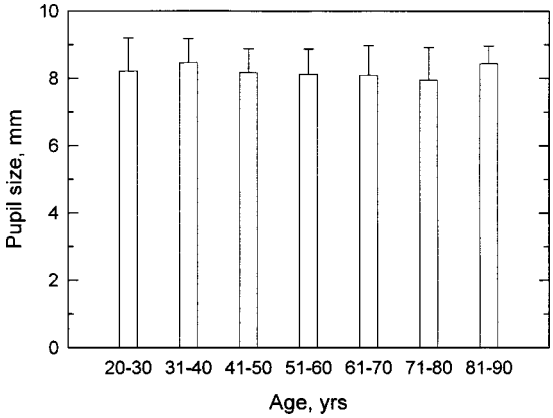


Fig. 18. Pupil sizes of subjects enrolled in the clinical trial, showing mean pupil diameter and standard deviation grouped in decades of age.

We considered whether nonretinal tissues of the eye could account for the decline in Raman signal intensity with age. Such decline could be due to either a change in carotenoid content in a nonretinal tissue or increased optical absorption of the ocular media. Other ocular tissues such as the lens, iris, ciliary body, and retinal pigment epithelium/choroid contain measurable amounts of various carotenoids by HPLC, whereas cornea, vitreous, and sclera do not;[56] but the concentrations relative to the macula are so much lower (at least one order of magnitude) that they are unlikely to exert any relevant effect. Moreover, control experiments on human cadaver eyes have shown that none of these nonretinal tissues yields any detectable carotenoid Raman signals at the illumination levels used in this study.[43]

It is known that optical absorption and scattering of the human ocular media increases with age and that these changes are due almost exclusively to the lens as opposed to the cornea, aqueous, or vitreous.[57,58] Vitreous scattering of light increases slightly with age in nondiabetic eyes when measured by dynamic light scattering and dark-field slit microscopy,[59] but this effect is not no-

ticeable clinically and is unlikely to interfere with our Raman measurements. The increasing absorption and scattering of blue–green light that occurs as the lens ages,[58,60–63] clearly could account for part of the decline in Raman signal with age. We excite with 488-nm laser light and measure backscattered light at 527 nm in the major C=C Raman peak. The average optical density ($T_L$) of the fully dilated noncataractous lens between age 20 and 60 can be estimated from the equation

$$T_L = 0.86T_{L1}[1 + 0.02(A - 32)],$$

where $A$ is the age in years and $T_{L1}$ is 0.187 at 490 nm and 0.120 at 530 nm.[63] This means that the total transmittance of the entering and exiting light during a Raman measurement would be 63% at age 20 and 39% at age 60, which could lead to a 38% reduction in signal, but we observe a >75% drop in average Raman measurement between ages 20 and 60. A more recent study suggests that increase in lens optical density with age is actually much more modest than previously reported; a substantial rise occurs only after age 60, and after cataract surgery and placement of a prosthetic intraocular lens, the average "lens-density index" of these postsurgical patients returns to the average level of a 20–30-year-old.[58]

The apparent decline of macular carotenoids with age as measured by *in vivo* resonance Raman spectroscopy is further supported by the fact that half of the study subjects over age 60 have prosthetic intraocular lenses that are designed to have high optical clarity in the visible range. Average Raman signals are not significantly different in pseudophakic patients relative to phakic patients ($P = 0.059$) older than 60, and even after cataract surgery their measured readings never approach the average level for a 20–30-year-old. In nine subjects with visually significant cataracts much denser than the lens changes seen in our normal subjects, we found an average rise ±S.D. of Raman counts from 90 ± 61 counts before surgery to 289 ± 130 counts after surgery, amounting to an increase of only 199 ± 128 counts. Direct comparison of our Raman technique with psychophysical heterochromatic flicker photometry and reflectometry techniques in the same population will be useful to confirm these findings.

It should be noted that there are substantial differences among the various technologies to measure macular pigment. Flicker photometry measures optical density at the edge of the illumination spot,[19] whereas the Raman method measures total carotenoids in the 1-mm-diameter area illuminated by the laser. Thus our Raman device in its current form would be unable to detect spatial alterations of macular pigment distribution that might occur with age or pathology.[64] Flicker photometry assumes that the carotenoid level is zero at a reference point in the perifovea[25] even though it is clear that significant levels of carotenoids are present throughout the peripheral retina,[17,18] whereas Raman measurement requires no such reference point. Flicker photometry relies on the assumption that the foveal retina has the same relative spectral sensitivity as the perifoveal area that is used to provide the baseline value,[24] but this assumption is complicated by the fact that the neural and photoreceptor organization of the retina varies dramatically with distance from the center of the fovea, and photopic sensitivity declines with age.[25,65] Resonance Raman spectroscopic measurement of macular carotenoids does not rely on this assumption, either.

Comparing Raman scattering with reflectometry and autofluorescence methods, we note that in addition to differing in spectral selectivity, the three methods also differ dramatically in the respective light paths used for fundus excitation and reflection. Shown schematically in Fig. 19 are the ocular media and fundus tissue layers to be considered. The Raman method uses light that is Raman backscattered directly from the macular pigment layer, which is positioned in the uppermost layer of the fundus. Therefore it does not have to rely, as is the case for the other two techniques, on light propagation through deeper fundus layers nor reflection at those layers or the sclera. In fact, any laser-excitation light transmitted through the macular pigment layer can be considered ineffective for a return-path Raman excitation in view of the high absorption and light scattering of the deeper fundus layers.

Fundus reflectometry measures macular pigment absorption indirectly by comparing highly complex fundus-reflectance spectra for two different fundus locations. The measuring light traverses all fundus layers twice, and the spectral fit needed for calculation of the pigment density relies on mathematical models of the respective *in-vivo* optical properties of the stratified fundus layers, all assumed to be homogeneous (absorption, reflection, and scattering strengths as well as spectral profiles). This situation could be problematic considering that all biological tissue layers, in particular irregularly distributed choroidal vessels and melanocytes in the choroidal stroma, are principally heterogeneous optical media.[27,28]

Autofluorescence appears to have an advantage over reflectometry in that it uses an indirect light source (lipofuscin) in the retinal epithelial layer for a single path measurement of macular pigments and thus avoids traversal of the deeper fundus tissue layers. However, like

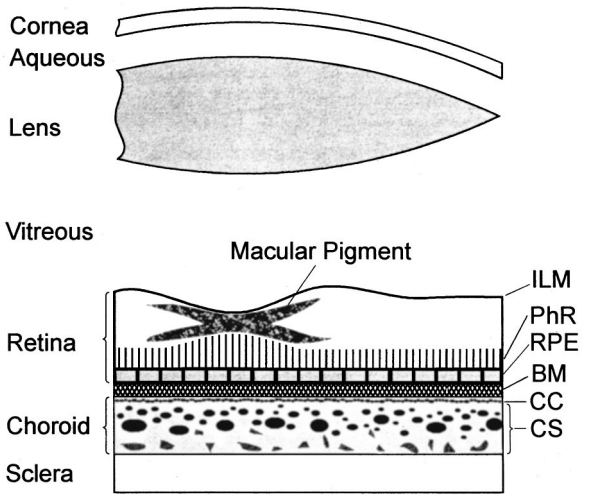


Fig. 19. Schematic representation of ocular media and fundus tissue layers (adapted from Ref. 28; not to scale). ILM, inner limiting membrane; PhR, photoreceptors; RPE, retinal pigment epithelium; BM, Bruch's membrane; CC, choriocapillaris; CS, choroidal stroma.

reflectometry it assumes a homogeneous distribution of tissue layers. Furthermore, it assumes that the fluorophore at the fovea is the same as that as at the perifovea and that foveal–perifoveal differences in absorption by other pigments located between the macular pigment and the fluorophore (retinal blood, visual pigments, retinal pigment epithelium melanin) are negligible.

If one assumes homogeneous optical properties of the tissue layers, reflectometry and autofluorescence detection methods do not require a correction for media absorption, unlike the Raman method in its current form, since the measurement at a reference location eliminates that contribution. The reference measurement also eliminates the effects of light loss by scattering and the effects of any neutral absorber or light loss such as from the pupil.

## 7. CONCLUSION

In conclusion, our results demonstrate that resonance Raman spectroscopy is a highly promising technology for the measurement of macular carotenoid levels in living humans. It is noninvasive, precise, sensitive, specific, rapid, reproducible, and objective. Our initial clinical studies have already identified an apparent decline in macular pigment levels during the normal aging process, although the magnitude of this decline remains uncertain since the Raman measurements require a correction factor for age-dependent ocular media opacity, a parameter that is not quantified for all tissues of the eye. Clinical trials involving a larger subject base with and without ocular pathology are under way and hold promise to help clarify the roles of lutein and zeaxanthin in the prevention and treatment of AMD and other blinding disorders.

## ACKNOWLEDGMENTS

The authors are grateful to Steve Wintch and Ninel Gregori for clinical use of the Raman instrument conducted at the Moran Eye Center of the University of Utah. This research was supported by funds from Spectrotek, L.C., the National Eye Institute [grants R29-EY11600, Small Business Technology Transfer STTR 1 R41 EY12324-01, and STTR 2 R42 EY12324-02], and Research to Prevent Blindness, Inc.

Address correspondence to W. Gellermann, Department of Physics, University of Utah, 115 S. 1400 E., Salt Lake City, Utah 84112; e-mail, werner@physics.utah.edu

## REFERENCES

1. R. A. Bone, J. T. Landrum, and S. L. Tarsis, "Preliminary identification of the human macular pigment," Vision Res. **25**, 1531–1535 (1985).
2. G. J. Handelman, D. M. Snodderly, A. J. Adler, M. D. Russett, and E. A. Dratz, "Measurement of carotenoids in human and monkey retinas," Methods Enzymol. **213**, 220–230 (1992).
3. W. Schalch, P. Dayhaw-Barker, and F. M. Barker, "The carotenoids of the human retina," in *Nutritional and Environmental Influences on the Eye*, A. Taylor, ed. (CRC, Boca Raton, Fla., 1999), pp. 215–250.
4. D. M. Snodderly, "Evidence for protection against age-related macular degeneration by carotenoids and antioxidant vitamins," Am. J. Clin. Nutr. Suppl. **62**, 1448S–1461S (1995).
5. Eye Disease Case Control Study Group, "Antioxidant status and neovascular age-related macular degeneration," Arch. Ophthalmol. (Chicago) **111**, 104–109 (1993).
6. J. M. Seddon, U. A. Ajani, R. D. Sperduto, R. Hiller, N. Blair, T. C. Burton, M. D. Farber, E. S. Gragoudas, J. Haller, D. T. Miller, L. A. Yannuzzi, and W. Willet, "Dietary carotenoids, vitamins A, C, and E, and advanced age-related macular degeneration," J. Am. Med. Assoc. **272**, 1413–1420 (1994).
7. B. R. Hammond, E. J. Johnson, R. M. Russell, N. I. Krinsky, K.-J. Yeum, R. B. Edwards, and D. M. Snodderly, "Dietary modification of human macular pigment density," Invest. Ophthalmol. Visual Sci. **38**, 1795–1801 (1997).
8. J. T. Landrum, R. A. Bone, H. Joa, M. D. Kilburn, L. L. Moore, and K. E. Sprague, "A one year study of the macular pigment: the effect of 140 days of a lutein supplement," Exp. Eye Res. **65**, 57–62 (1997).
9. J. T. Landrum, R. A. Bone, and M. D. Kilburn, "The macular pigment: a possible role in protection from age-related macular degeneration," Adv. Pharmacol. **38**, 537–556 (1997).
10. R. A. Bone, J. T. Landrum, S. T. Mayne, C. M. Gomez, S. E. Tibor, and E. E. Twaroska, "Macular pigment in donor eyes with and without AMD: a case-control study," Invest. Ophthalmol. Visual Sci. **42**, 235–240 (2000).
11. Age Related Eye Disease Study Research Group, "A randomized, placebo controlled clinical trial of high-dose supplementation with vitamins C and E, beta carotene, and zinc for age-related macular degeneration and vision loss," Arch. Ophthalmol. **119**, 1417–1436 (2001).
12. D. M. Snodderly, J. D. Auran, and F. C. Delori, "The macular pigment, I: absorbance spectra, localization, and discrimination from other yellow pigments in primate retinas," Invest. Ophthalmol. Visual Sci. **25**, 660–673 (1984).
13. R. A. Bone, J. T. Landrum, L. Fernandez, and S. L. Tarsis, "Analysis of macular pigment by HPLC: retinal distribution and age study," Invest. Ophthalmol. Visual Sci. **29**, 843–849 (1988).
14. R. A. Bone, J. T. Landrum, L. M. Friedes, C. A. Gomez, M. A. Kilburn, E. Menendez, I. Vidal, and W. Wang, "Distribution of lutein and zeaxanthin stereoisomers in the human retina," Exp. Eye Res. **64**, 211–218 (1997).
15. D. M. Snodderly, G. J. Handelman, and A. A. Adler, "Distribution of individual macular pigment carotenoids in central retina of macaque and squirrel monkeys," Invest. Ophthalmol. Visual Sci. **32**, 268–279 (1991).
16. J. D. M. Gass, "The Müller cell cone, an overlooked part of the anatomy of the fovea centralis," Arch. Ophthalmol. **117**, 821–823 (1999).
17. O. G. Sommerberg, W. G. Siems, J. S. Hurst, J. W. Lewis, D. S. Kliger, and F. J. van Kuijk, "Lutein and zeaxanthin are associated with photoreceptors in the human retina," Curr. Eye Res. **19**, 502–505 (1999).
18. L. M. Rapp, S. S. Maple, and J. H. Choi, "Lutein and zeaxanthin concentrations in rod outer segment membranes from perifoveal and peripheral human retina," Invest. Ophthalmol. Visual Sci. **41**, 1200–1209 (2000).
19. B. R. Hammond, Jr., B. R. Wooten, and D. M. Snodderly, "Individual variations in the spatial profile of human macular pigment," J. Opt. Soc. Am. A **14**, 1187–1196 (1997).
20. P. S. Bernstein and N. B. Katz, "The role of ocular free radicals in age-related macular degeneration," in *Environmental Stressors: Effects on Lung, Skin, Eye and Immune System Function*, J. Fuchs and L. Packer, eds. (Marcel Dekker, New York, 2000), pp. 423–456.
21. S. Beatty, H.-H. Koh, D. Henson, and M. Boulton, "The role of oxidative stress in the pathogenesis of age-related macular degeneration," Surv. Ophthalmol. **45**, 115–134 (2000).
22. V. M. Reading and R. A. Weale, "Macular pigment and chromatic aberration," J. Am. Optom. Assoc. **64**, 231–234 (1974).
23. S. Beatty, I. J. Murray, D. B. Henson, D. Carden, H.-H. Koh, and M. E. Boulton, "Macular pigment and risk for age-related macular degeneration in subjects from a northern

European population," Invest. Ophthalmol. Visual Sci. **42**, 439–446 (2001).
24. D. M. Snodderly and B. R. Hammond, "*In vivo* psychophysical assessment of nutritional and environmental influences on human ocular tissues: lens and macular pigment," in *Nutritional and Environmental Influences on the Eye*, A. Taylor, ed. (CRC, Boca Raton, Fla., 1999), pp. 251–273.
25. J. S. Werner, M. L. Bieber, and B. E. Schefrin, "Senescence of foveal and parafoveal cone sensitivities and their relations to macular pigment density," J. Opt. Soc. Am. A **17**, 1918–1932 (2000).
26. B. R. Hammond and M. Caruso-Avery, "Macular pigment optical density in a southwestern sample," Invest. Ophthalmol. Visual Sci. **41**, 1492–1497 (2000).
27. D. van Norren and L. F. Tiemeijer, "Spectral reflectance of the human eye," Vision Res. **26**, 313–320 (1986).
28. F. C. Delori and K. P. Pflibsen, "Spectral reflectance of the human ocular fundus," Appl. Opt. **28**, 1061–1077 (1989).
29. J. van de Kraats, T. T. J. M. Berendshot, and D. van Norren, "The pathways of light measured in fundus reflectometry," Vision Res. **36**, 2229–2247 (1996).
30. T. Berendshot, J. van de Kraats, and D. van Norren, "Three methods to measure macular pigment compared in a lutein intake study," Invest. Ophthalmol. Visual Sci. Suppl. **39**, S314 (1999).
31. P. E. Kilbride, K. R. Alexander, M. Fishman, and G. A. Fishman, "Human macular pigment assessed by imaging fundus reflectometry," Vision Res. **29**, 663–674 (1989).
32. R. H. Webb, G. W. Hughes, and O. Pomerantzeff, "Flying spot TV ophthalmoscope," Appl. Opt. **19**, 2991–2997 (1980).
33. R. W. Webb, G. W. Hughes, and F. C. Delori, "Confocal scanning laser ophthalmosope," Appl. Opt. **26**, 1492–1499 (1987).
34. D. van Norren and J. van de Kraats, "Imaging retinal densitometry with a confocal scanning ophthalmoscope," Vision Res. **29**, 1825–1830 (1989).
35. A. E. Elsner, S. A. Burns, F. C. Delori, and R. H. Webb, "Quantitative reflectometry with the SLO," in *Laser Scanning Ophthalmoscopy and Tomography*, J. E. Nasemann and R. O. W. Burk, eds. (Quintessenz-Verlag, Berlin, 1990), pp. 109–121.
36. A. E. Elsner, S. A. Burns, G. W. Hughes, and R. H. Webb, "Reflectometry with a scanning laser ophthalmoscope," Appl. Opt. **31**, 3697–3710 (1992).
37. A. E. Elsner, S. A. Burns, E. Beausencourt, and J. J. Weiter, "Foveal cone photopigment distribution: small alterations associated with macular pigment distribution," Invest. Ophthalmol. Visual Sci. **39**, 2394–2404 (1998).
38. D. Schweitzer, M. Hammer, and M. Scibor, "Imaging spectrometry in ophthalmology: principle and applications in microcirculation and in investigation of pigments," Invest. Ophthalmol. Visual Sci. **39**, 2001–2011 (1998).
39. F. C. Delori, "Macular pigment density measured by reflectometry and fluorophotometry," in *Ophthalmic and Visual Optics and Noninvasive Assessment of the Visual System*, Vol. 3 of 1993 OSA Technical Digest Series (Optical Society of America, Washington, D.C., 1993), pp. 240–243.
40. F. C. Delori, D. G. Goger, B. R. Hammond, D. M. Snodderly, and S. A. Burns, "Macular pigment density measured by autofluorescence spectrometry: comparison with reflectometry and heterochromatic flicker photometry," J. Opt. Soc. Am. A **18**, 1212–1230 (2001).
41. T. T. J. M. Berendshot, R. A. Goldbohm, W. A. A. Kloepping, J. van de Kraats, J. Van Norel, and D. van Norren, "Influence of lutein supplementation on macular pigment, assessed with two objective techniques," Invest. Ophthalmol. Visual Sci. **41**, 3322–3326 (2000).
42. W. Gellermann, M. D. Yoshida, R. W. McClane, N. Balashov, and P. S. Bernstein, "Raman detection of pigments in the human retina," in *Optical Biopsy II*, R. R. Alfano and A. Katzir, eds., Proc. SPIE **3250**, 8–17 (1998).
43. P. S. Bernstein, M. D. Yoshida, N. B. Katz, R. W. McClane, and W. Gellermann, "Raman detection of macular carotenoid pigments in intact human retina," Invest. Ophthalmol. Visual Sci. **39**, 2003–2011 (1998).
44. I. V. Ermakov, R. W. McClane, W. Gellermann, and P. S. Bernstein, "Resonant Raman detection of macular pigment levels in the living human retina," Opt. Lett. **26**, 202–204 (2001).
45. P. S. Bernstein, W. Gellermann, and R. W. McClane, "Measurement of macular carotenoid levels in the human retina using Raman spectroscopy," U.S. patent 5,873,831, February 23, 1999.
46. W. Gellermann, R. W. McClane, N. B. Katz, and P. S. Bernstein, "Method and apparatus for noninvasive measurement of carotenoids and related chemical substances in biological tissue," U.S. patent 6,205,354, March 20, 2001.
47. T. R. Hata, T. A. Scholz, I. V. Ermakov, R. W. McClane, F. Khachik, W. Gellermann, and L. K. Pershing, "Noninvasive Raman spectroscopic detection of carotenoids in human skin," J. Invest. Dermatol. **115**, 441–448 (2000).
48. A. P. Shreve, J. K. Trautman, T. G. Owens, and A. C. Albrecht, "Determination of the S2 lifetime of $\beta$-carotene," Chem. Phys. Lett. **178**, 89 (1991).
49. Y. Koyama, I. Takatsuka, M. Nakata, and M. Tasumi, "Raman and infrared spectra of the all-*trans*, 7-*cis*, 9-*cis*, 13-*cis*, and 15-*cis* isomers of $\beta$-carotene: key bands distinguishing stretched or terminal-bent configurations from central-bent configurations" J. Raman Spectrosc. **19**, 37–49 (1988).
50. A. C. Albrecht, "On the theory of Raman intensities," J. Chem. Phys. **34**, 1476–1484 (1961).
51. W. Kiefer and M. Spiekermann, "Resonance Raman theories," in *Infrared and Raman Spectra*, B. Schrader, ed. (VCH Verlagsgesellschaft, Weinheim, Germany, 1995), pp. 468–473.
52. F. C. Delori, J. S. Parker, and M. A. Mainster, "Light levels in fundus photography and fluorescein angiography," Vision Res. **20**, 1099–1104 (1980).
53. American National Standards Institute, "American national standard for safe use of lasers," ANSI Z136.1-2000 (Laser Institute of America, Orlando, Fla., 2000), Sec. 8.3.
54. L. Apt and A. Henrick, "Pupillary dilatation with single eyedrop mydriatic combinations," Am. J. Ophthalmol. **89**, 553–559 (1980).
55. C. J. Hammond, H. Sneider, T. D. Spector, and C. E. Gilbert, "Factors affecting pupil size after dilatation: the Twin Eye Study," Br. J. Ophthamol. **84**, 1173–1176 (2000).
56. P. S. Bernstein, F. Khachik, L. S. Carvalho, G. J. Muir, D. Y. Zhao, and N. B. Katz, "Identification and quantitation of carotenoids and their metabolites in the tissues of the human eye," Exp. Eye Res. **72**, 215–223 (2001).
57. E. A. Boettner and J. R. Wolter, "Transmission of the ocular media," Invest. Ophthalmol. Visual Sci. **1**, 776–783 (1962).
58. P. A. Sample, F. D. Esterson, R. N. Weinreb, and R. M. Boynton, "The aging lens: *in vivo* assessment of light absorption in 84 human eyes," Invest. Ophthalmol. Visual Sci. **29**, 1306–1311 (1988).
59. J. Sebag, R. R. Ansari, S. Dunker, and K. I. Suh, "Dynamic light scattering of diabetic vitreopathy," Diabetes Technol. Ther. **1**, 169–176 (1999).
60. J. Dillon, L. Zheng, J. C. Merriam, and E. R. Gaillard, "Transmission spectra of light to the mammalian retina," Photochem. Photobiol. **71**, 225–229 (2000).
61. E. R. Gaillard, L. Zheng, J. C. Merriam, and J. Dillon, "Age-related changes in the absorption characteristics of the primate lens," Invest. Ophthalmol. Visual Sci. **41**, 1454–1459 (2000).
62. R. A. Weale, "Age and the transmittance of the human crystalline lens," J. Physiol. **395**, 577–587 (1988).
63. J. Pokorny, V. C. Smith, and M. Lutze, "Aging of the human lens," Appl. Opt. **26**, 1437–1440 (1987).
64. A. E. Elsner, S. A. Burns, J. J. Weiter, and F. C. Delori, "Infrared imaging of subretinal structures in the human ocular fundus," Vision Res. **36**, 191–201 (1996).
65. B. R. Hammond, B. R. Wooten, and D. M. Snodderly, "Preservation of visual sensitivity of older subjects: association with macular pigment density," Invest. Ophthalmol. Visual Sci. **39**, 397–406 (1998).